

## **EXAMINATION OF CAVITATION EROSION PARTICLES MORPHOLOGY IN CORROSIVE WATERS**

---

**S. A. Karrab**

Mining and Metallurgical Engineering Department, Assiut University, Assiut71516,  
Egypt

e-mail: [sgarrab2005@yahoo.co.uk](mailto:sgarrab2005@yahoo.co.uk)

**M. A. Doheim**

Mining and Metallurgical Engineering Department, Assiut University, Assiut71516,  
Egypt

e-mail: [mohdoheim@yahoo.com](mailto:mohdoheim@yahoo.com)

**Mohammed S. Aboraia**

Mining and Metallurgical Engineering Department, Assiut University, Assiut71516,  
Egypt

e-mail: [maboraia@hotmail.com](mailto:maboraia@hotmail.com)

**S.M. Ahmed**

Mechanical Engineering Department, Majmaah University, SA

e-mail: [shemy2007@yahoo.com](mailto:shemy2007@yahoo.com)

(Received June 27, 2012 Accepted September 11, 2012)

### **Abstract**

Wear particles produced by vibratory cavitation erosion tests on 1045 carbon steels in three different corrosive media: distilled water, tap water and 3 % NaCl water were analyzed. Scanning electron microscope (SEM) of wear particles were acquired, forming database for further analysis. This study shows that there is no remarkable difference in the particle size with test solution. However, the frequency distribution of particle sizes differed with the test solution. It is the highest at small sizes for tap and distilled water. While for salt water, it is the highest for the larger sizes (larger than 50  $\mu\text{m}$ ). All the particles, irrespective of solution, manifested similar morphological features such as lamellar shape, crack propagation on the particle surface and secondary cracks. This indicates that the particles are produced by a single mechanism, namely, fatigue. With regard to the role of corrosion in the development of cavitation erosion, it was most pronounced in the case of salt water. It was found that dissolution of ferrite acts as areas of stress concentration which give rise to crack initiations. This gives a strong impetus to the crack initiations.

**Keywords:** Cavitation erosion-corrosion, particle morphology, fatigue, carbon steel, corrosive waters.

## 1. Introduction

Cavitation erosion-corrosion results from the interaction of mechanical and chemical phenomena, which involve material removal from mechanically eroded surfaces exposed to corrosive liquids. The mechanical erosion processes originate through events occurring either in flowing or in vibrating fluid media: nucleation, growth and collapse in high pressure regions. During the bubble collapse, a large pulse of stress is generated and this is accompanied by a shock wave and/or microjet that impinges the solid surface in contact with liquid. A consensus has developed that material removal in multiple impact situations (e.g., cavitation erosion, liquid droplet erosion and solid-particle erosion) is not a result of single impulses or impacts. That is, damage accumulates over thousands of impacts before a particle is dislodged as discussed elsewhere [1, 2]. Based on microscopic studies of surface damage and dislodged particles from different materials cavitated in different liquids, Ahmed et al. [3-8] have found that the predominant failure mode in cavitation erosion is fatigue. Abouel-kasem et al [7] studied the cavitation erosion pits and their effects on erosion progression for four materials by means of vibratory erosion. They observed two kinds of pits formed on specimen surfaces, one by microjet impact and the other by shockwave blow. Their systematic observations for the feature of microjet-pits with the testing time showed that the sizes and shapes of microjet-pits did not change at all and such pits scarcely played an important role in developing the erosion.

Most structural materials either corrode in aqueous fluids or owe their stability to the presence of a passive film. In general, cavitation is likely to enhance the dissolution of the former alloy and reduce or eliminate passivity of the later. Consequently, cavitation erosion usually has a corrosive component in aqueous fluids which may be a minor or major factor depending on the combination of metal(s) and fluid and on the intensity of cavitation [9]. The cavitation erosion-corrosion has been investigated in the literature [10-15]. It is reported that conjoint action of electrochemical and mechanical factors produce far more damage than if each acted separately. Most measurements of such synergistic effect are based on the weight loss scale. From the view of the authors, this is helpful in screening the material resistance and cannot clearly explain the cavitation erosion-corrosion mechanism(s). In a trial by the authors [16] to elucidate the erosion-corrosion mechanism(s), they tested carbon steel in distilled water, tap water and 3 % NaCl water. The eroded surfaces in the early stages, i.e. the event of damage is isolated, have been systematically examined using SEM. They observed three kinds of pits formed on the eroded surface. Corrosion pits have a lamella structure and have a large size of 100  $\mu\text{m}$  for salt water. For distilled and tap water, the corrosion pits were superficial in appearance. However for NaCl water, the corrosion pits appeared to be the deepest. The second kinds of pits were erosion pits that were formed by microjet impact and have a size of few micrometers. The third kind was the erosion-corrosion pits, where the corroded areas act as favorite sites for gathering the erosion pits. The authors [17] investigated also the ring areas formed around the cavitation erosion pits on the surface of carbon steel. They found that the ring areas formed around micropits are the result of corrosion effect and are not the result of thermal effects due to bubble collapse [18,19].

Wear particle analysis is a widespread and a powerful technique that can be used to characterize the tribological condition of mechanical systems [20]. The most relevant

feature in such analysis includes size, shape, surface texture, edge detail and thickness ratio [21]. The particle characteristics are sufficiently specific so that the operating wear modes within an equipment may be described, allowing prediction of the behavior of the machine [22]. Accordingly, the proper action that might be considered is to correct the abnormal wear mode and to prevent costly secondary damage.

The studies on cavitation erosion from the particle analysis point of view are relatively few [23-26]. Recently, Ahmed and his colleague run a research program on the analysis of cavitation erosion particles for different materials, different liquids and different liquid parameters [6-8, 27, 28]. Their main conclusions were: (1) the dominant mode of cavitation failure for ductile material is fatigue irrespective of temperature, test liquids, and test time, (2) the particles removed during the incubation period have a distinctive characteristics that can be used as a monitor for early detection of cavitation erosion closed systems, (3) the pits formed by microjet impact scarcely played an important role in developing erosion. In context, the particles generated by cavitation erosion in corrosive media are scarcely studied according to the authors knowledge.

The present investigation aims to analyze quantitatively and qualitatively the particles generated by cavitation erosion of 1045 carbon steel in three media, namely: distilled water, tap water and 3% NaCl water. In the light of particles analysis and examination of eroded surface, the cavitation erosion-corrosion is highlighted.

## **2. Experimental**

Cavitation experiments were carried out using a well-known and widely used vibratory system [29, 30]. A schematic diagram of the test equipment is shown in Fig.1. The device consists of a piezoelectric transducer oscillating at  $20 \text{ kHz} \pm 50\text{Hz}$  frequency and an exponential horn which amplifies the vibration amplitude. The horn tip was made of a cavitation resistant material and it had a flat head as well as its dimensions are shown in Fig. 1(b). The specimen was placed coaxially with the horn and was held stationary at the distance  $L$  from the horn tip as shown in Fig.1(a). The flat face of the vibrating tip generates suction during its upward motion under liquid, which results in the creation of vapor-filled bubbles collectively known as a cavitation zone. That zone collapses during the subsequent downward motion. Cavitation damage occurs on the vibrating tip and on the stationary specimen. However, the damage that occurs on the horn tip is negligible compared with that occurs on the stationary one. Thus peak-to-peak amplitude of vibration of the horn tip was  $50 \mu\text{m}$ . The separation distances  $L$  between the specimen and the end of vibrating tip was initially adjusted using dial gage and maintained at the value of  $0.8 \text{ mm}$ , in the present study, to obtain significant values of erosion rates [31]. This experimental procedure is conforming to ASTM standard G32-09 [32].

Distilled water, tap water and 3% solution of NaCl in distilled water are used as cavitating liquids. The salt water solution was made with reagent grade NaCl. The specimen and the end of the horn tip were immersed in 1200 ml open beaker, containing 700 ml of the test liquid. Since the temperature change will affect the physical properties of the test liquid such as dissolved gas, pH, surface tension and vapor pressure, the degree of erosion [8] and corrosion [33] as well as their interaction will be undoubtedly changed. Therefore, the test liquid temperature was kept constant at  $27 \pm 1 \text{ }^\circ\text{C}$ , by circulating cooling water around the beaker, as shown in Fig.1(a).

Preliminary tests showed that temperature of the liquid film on the specimen surface rose rapidly. Regardless of the constant temperature in the beaker, this temperature is measured for a maximum duration test time with a thermocouple inserted in the center of test piece. It was found for 10 min. (maximum interval test time), that the film temperature did not exceed the controlled temperature of beaker by more than 2 °C.

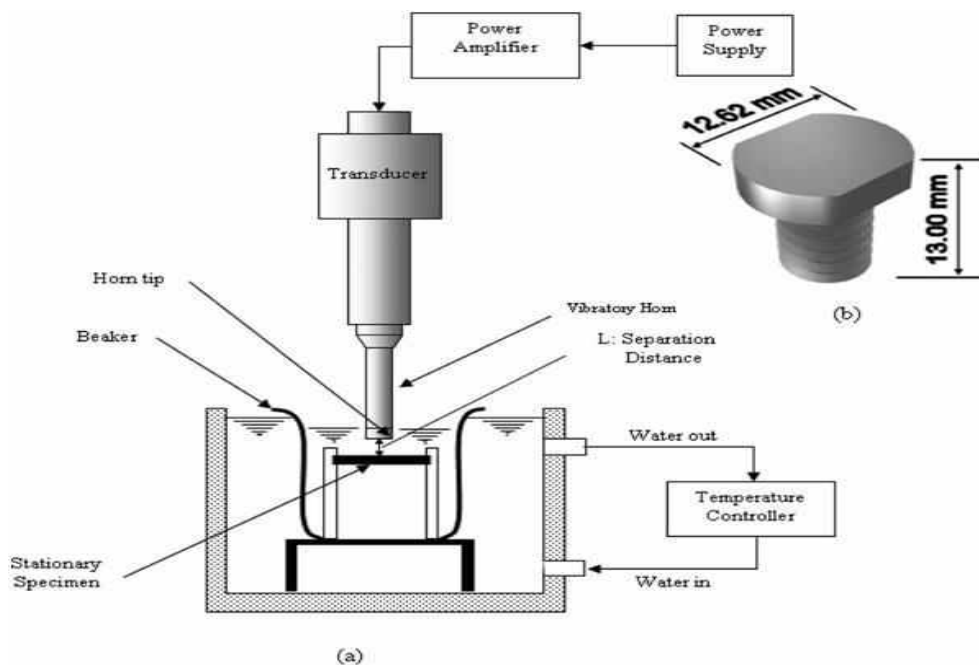


Fig.1. (a) schematic diagram of the test equipment, (b) horn's tip

The specimens were made of AISI-1045 carbon steel whose corrosion damage is easily detectable because of its low-corrosion resistance. The chemical composition and the mechanical properties are listed in Tables [1] and [2] [34]. The metallographic structure of AISI 1045 carbon steel is given in Fig.2. The microstructure composes of (white) pearlite and (dark) ferrite. The specimens were flat-surfaced discs of 14mm in diameter and 10mm height and were cut from a single rod (as cast) to ensure metallurgical uniformity. Since the surface roughness plays an important role in developing the erosion and material removal [3], therefore, the specimen's working faces were polished with grade 3000 dry emery paper to ensure average roughness  $R_a$  within 0.08  $\mu\text{m}$ . Before and after each test, the specimens were rinsed in acetone and dried in air and weighed with a 100 g  $\pm 0.1$  mg sensitivity balance.

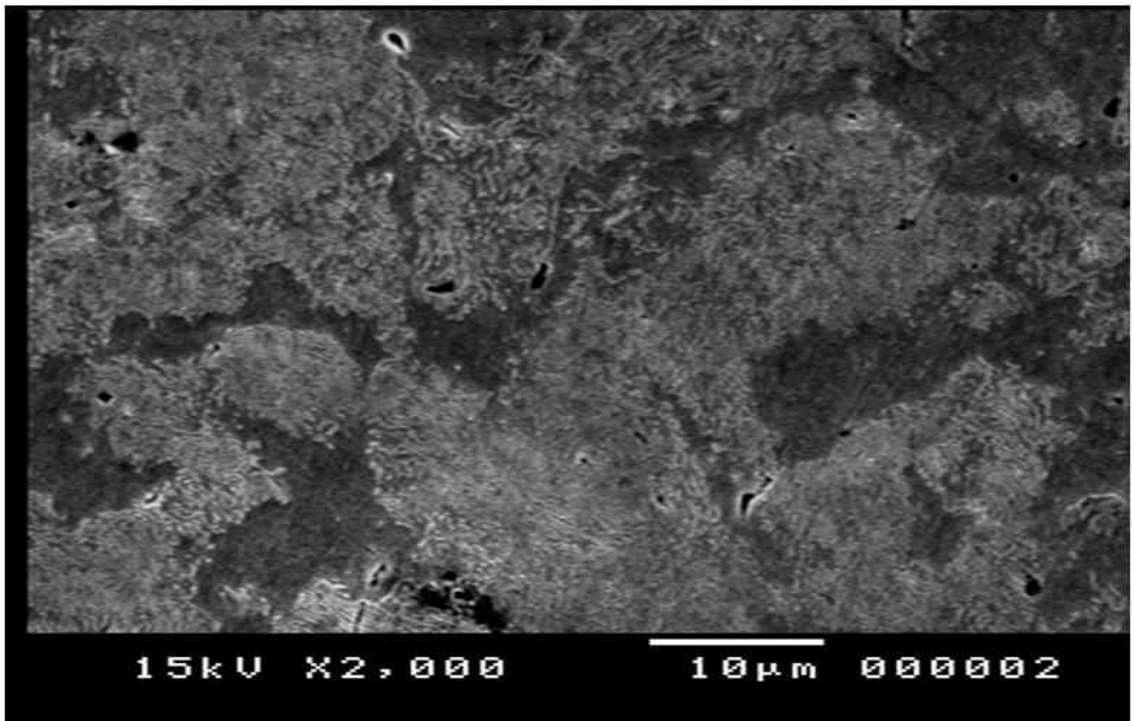


Fig.2. SEM photograph showing the microstructure of steel AISI-1045 with (white) pearlite and (dark) ferrite

**Table (1) Chemical Composition of mild steel**

Carbon (C)	Silicon (Si)	Manganese (Mn)	Phosphorus (P)	Sulphur (S)
0.42% – 0.48%	0.15% – 0.45%	0.6% – 0.9%	0.030% Max	0.035% Max

**Table (2) mechanical properties of mild steel**

Density kg/m <sup>3</sup>	Young's Modulus GPa	Tensile Strength MPa	Yield Strength MPa	Elastic Modulus GPa	Poisson's Ratio	Brinell Hardness HB	Reduction in Area (%)
7700-8030	190-210	569 Standard	343 Standard	190-210	0.27-0.30	160-220 Annealed	45

The wear particles were collected from the test solutions at the end of each test and for test time of 20, 30, 40, 50 min. The eroded particles were separated from the test solutions by using a ferrographic technique. Figure 3 shows the schematic diagram of the ferrograph. Since the wear is a heterogeneous process, the test solution contained

both very large and small particles. The solution is repeatedly poured at the top of the slide to collect all possible eroded particles. The particles are placed on a brass stub covered with carbon tape. Then, the morphology and chemical composition of particles were examined using SEM (JEOL JSM 5400) equipped with an energy-dispersive X-ray microanalyzer. Using the SEM images of particles and the image processing system image-J software, the particles were characterized in terms of area (A), equivalent diameter (d), perimeter (P), elongation ratio (EL), and roundness ( $P^2/4\pi A$ ).

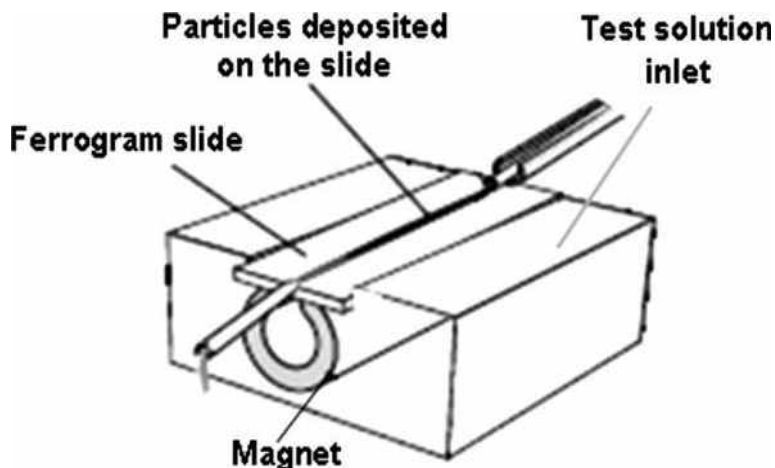


Fig. 3. Schematic diagram of the ferrograph

### 3. Results and Discussion

As soon as possible, the particles were immediately removed from the solution after the test to limit their corrosion. However, in salt solution it was observed that the number of wear particles (Wp) were the less as shown in Fig. 4. This is in contradiction with the corrosive action observed for the eroded surfaces and the weight loss [14] and as will be illustrated in next section 3.3. On the other hand it was found that the salt crystals (Cs) were massively formed as shown in Fig.4. The salt crystals are arranged in fixed geometric patterns or lattices. They have an ordered arrangement of units maximizing the space they occupy. The higher symmetry of structural units and the weaker the forces that are between them, the more likely and more rapidly crystallization occurs as shown in Fig. 5. Many of these crystals were formed on the particles, which tended to obscure these particles and cannot be observed by SEM. To overcome this problem, the salt solution was diluted by distilled water since supersaturation can lead to form crystals.

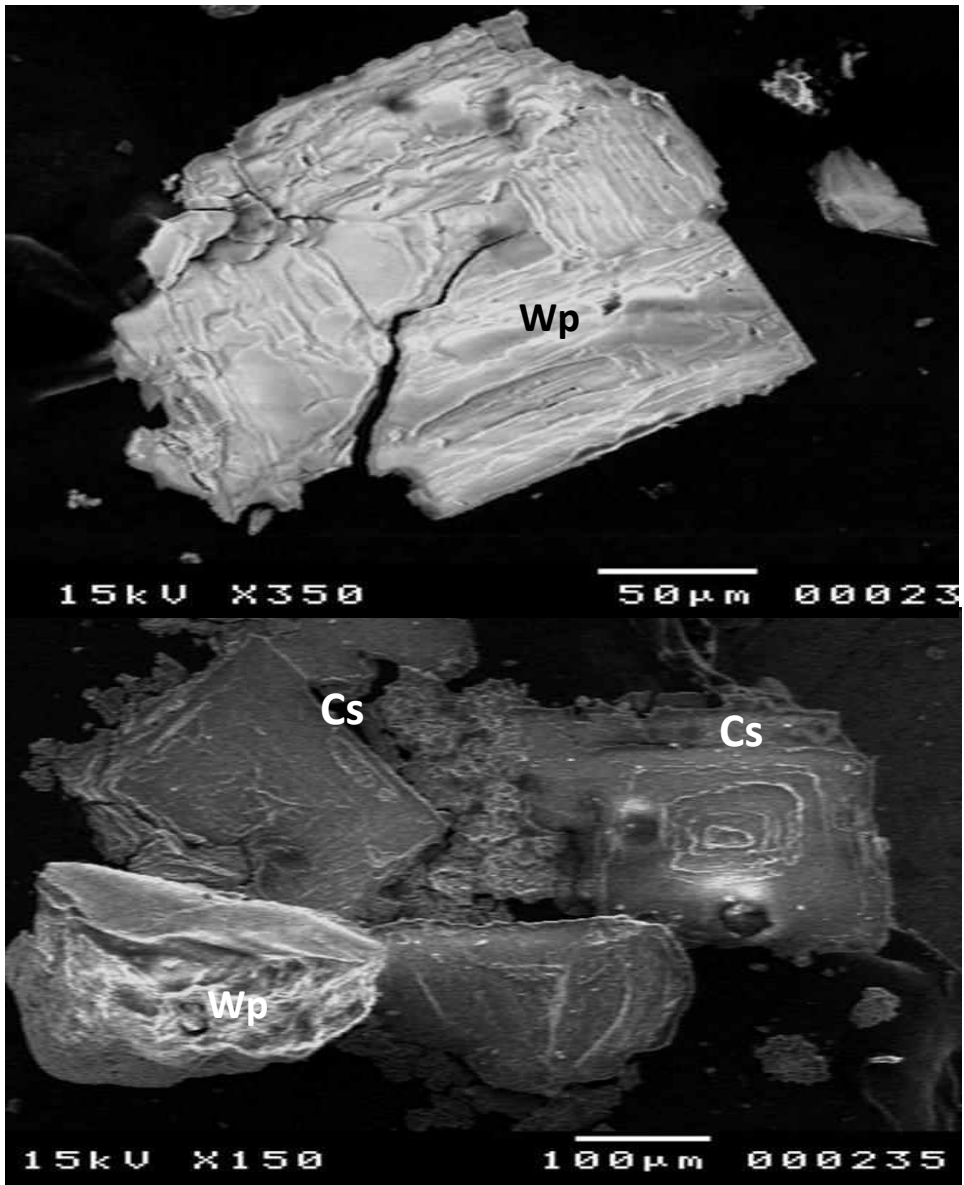
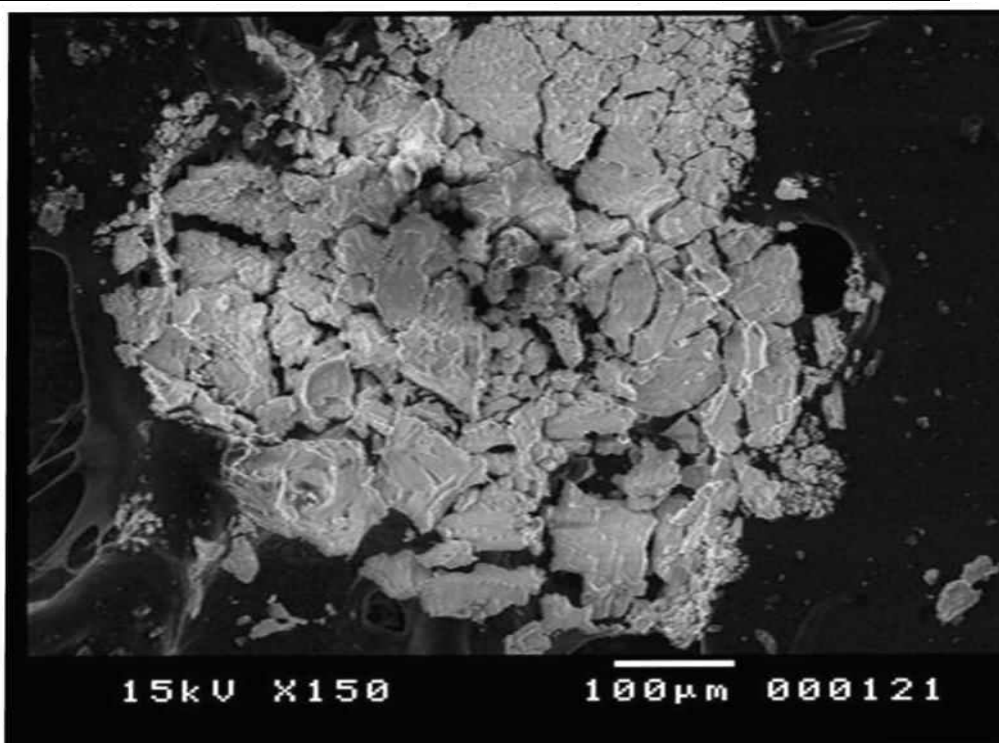


Figure 4, SEM photos illustrating dominant salt crystals over cavitated particles in salt solution.



**Fig. 5. SEM photo illustrating crystallization of NaCl crystals (Cs) over the cavitated particles**

### *3.1 Particle morphology and erosion mechanism*

Figures 6 and 7 show typical particles observed for different test liquids and for test times of 20 and 30 min, respectively. It is worth noting that these particles are generated during the incubation period. It is observed from these photographs that the particle size is comparable and that the particle shape is irregular for all the test waters. The dislodged particles have different sizes. There are small sizes (a few micrometers) and large sizes (about 300  $\mu\text{m}$ ), but it is focused in this section on the large sizes for ease of examination and analysis. The photographs illustrate that all the generated particles at the incubation period are laminar particles and show signs of plastic deformation. Closer observation of these particles show that most of these particles retain what appeared to be a part of the original face of the specimen, labeled V in the figures, and which may be distinguished by polishing traces. The corrosive debris were often found adhering to the surface of particles. It is to be noted that on the salt-water-particles, there is no corrosion product adhering to them. This is because of the salt solution, containing the particles, was diluted by distilled water to remove the formation of the salt crystals as mentioned above. These particles morphological features are in consistent with that reported by Abouel-kasem et al. [6-8 and 27] for different ductile materials and different test conditions [16].

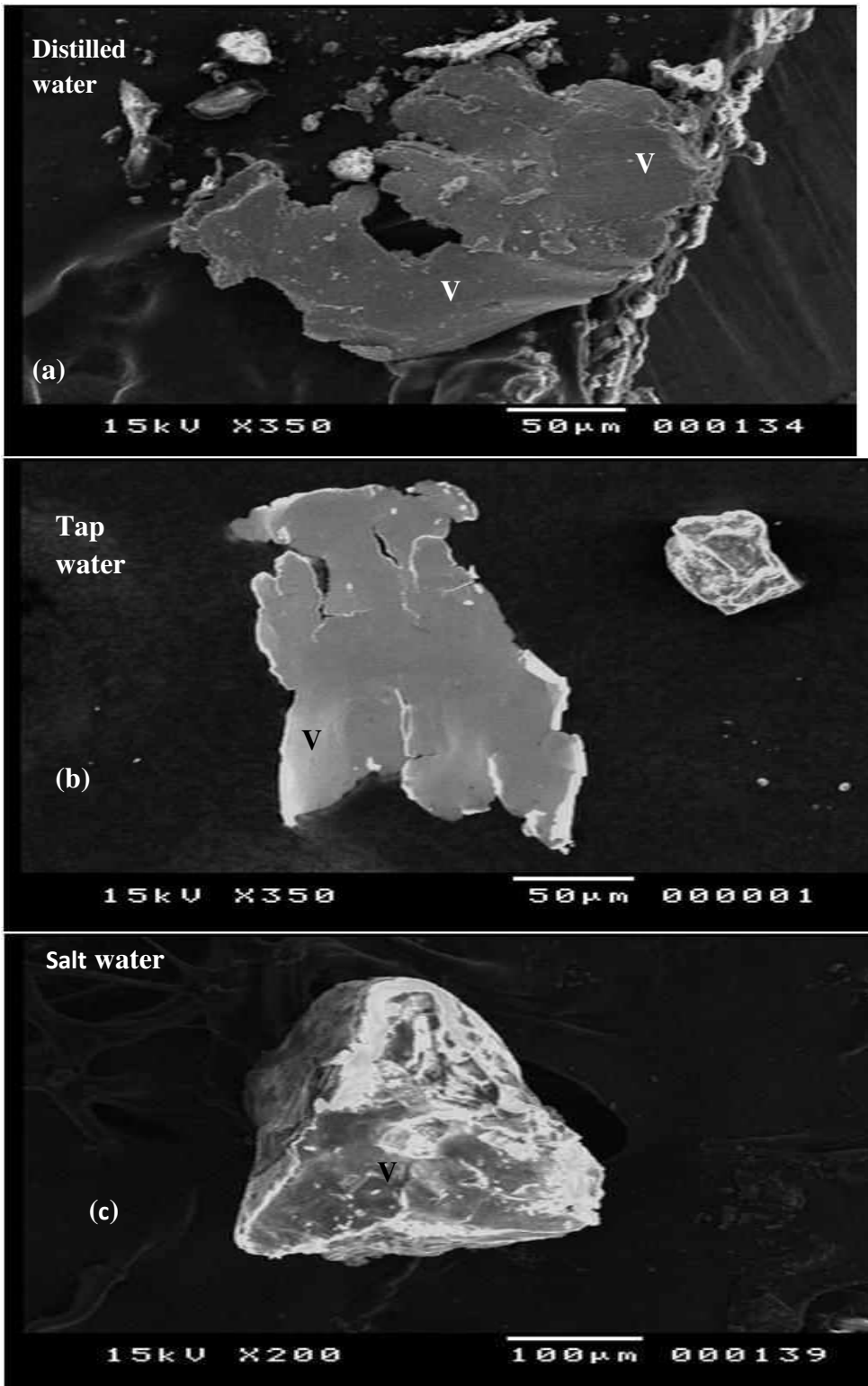


Fig. 6 SEM Photographs of particles removed for 1045 carbon steel cavitating in different water at test time of 20 min.

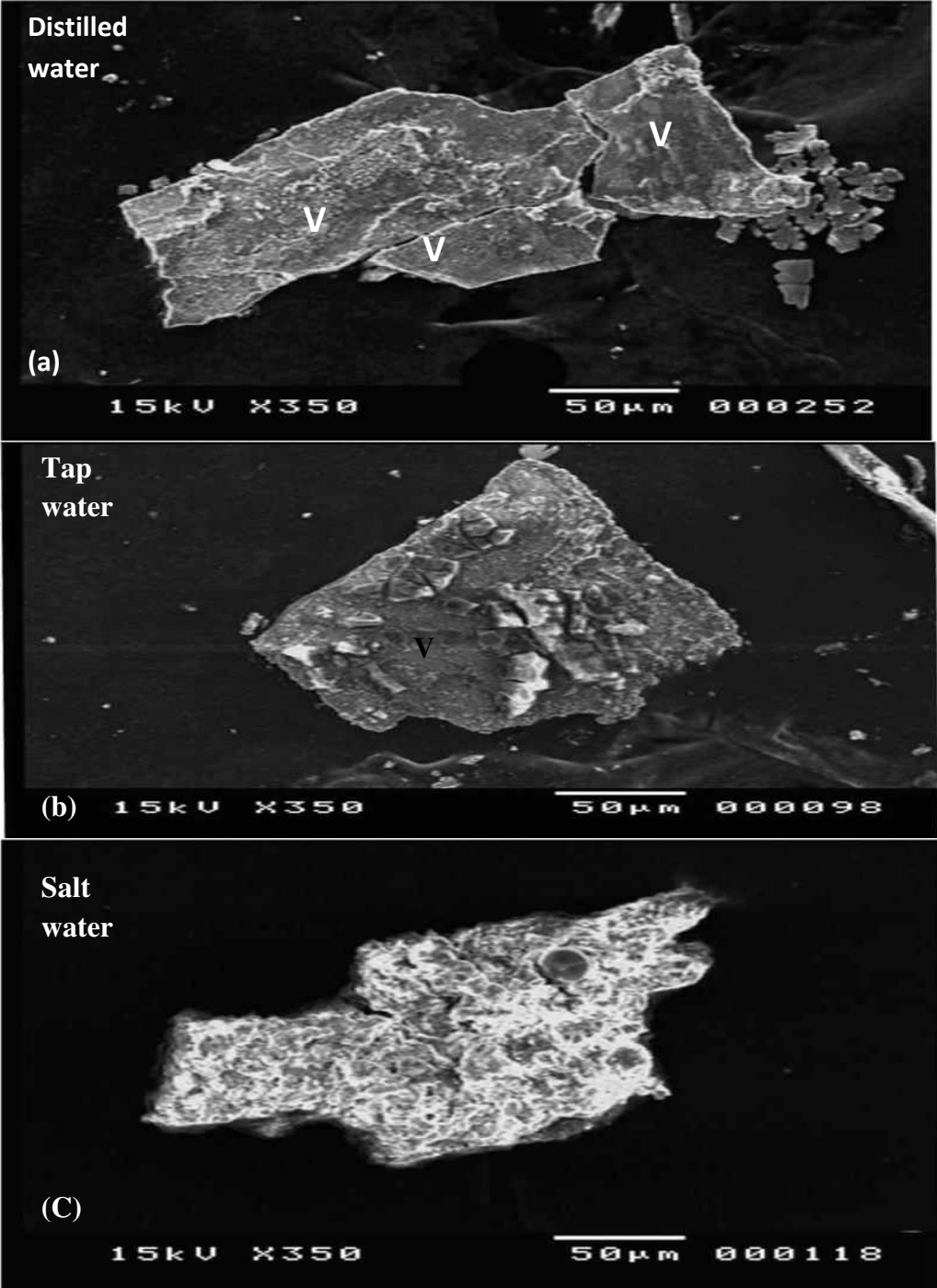


Fig.7 SEM photographs of particles from 1045 carbon steel cavitating in different waters and at test time of 30 min

The topography of the detached particles is a negative replica corresponding to that of cavitation damage surface. Therefore, surface examination of wear particles is clearly a reliable technique for predicting the cavitation erosion-corrosion mechanism. The features of particles mentioned above illustrates that large and small particles, irrespective of test solution, showed very similar morphological characteristics, which proves that they were formed by the same mechanism. To shed more light on the similarity of particle features, high magnifications for a typical particle formed in different waters are given in Fig.8. All the particles at different waters and times showed signs of plastic deformation. It is easy to observe the secondary crack, crack propagation and ridge shown on the surface of all the particles depicted on Figs. 6 and 7. This gives evidence that the predominant mode of cavitation failure for ductile material is fatigue failure irrespective of test solutions.

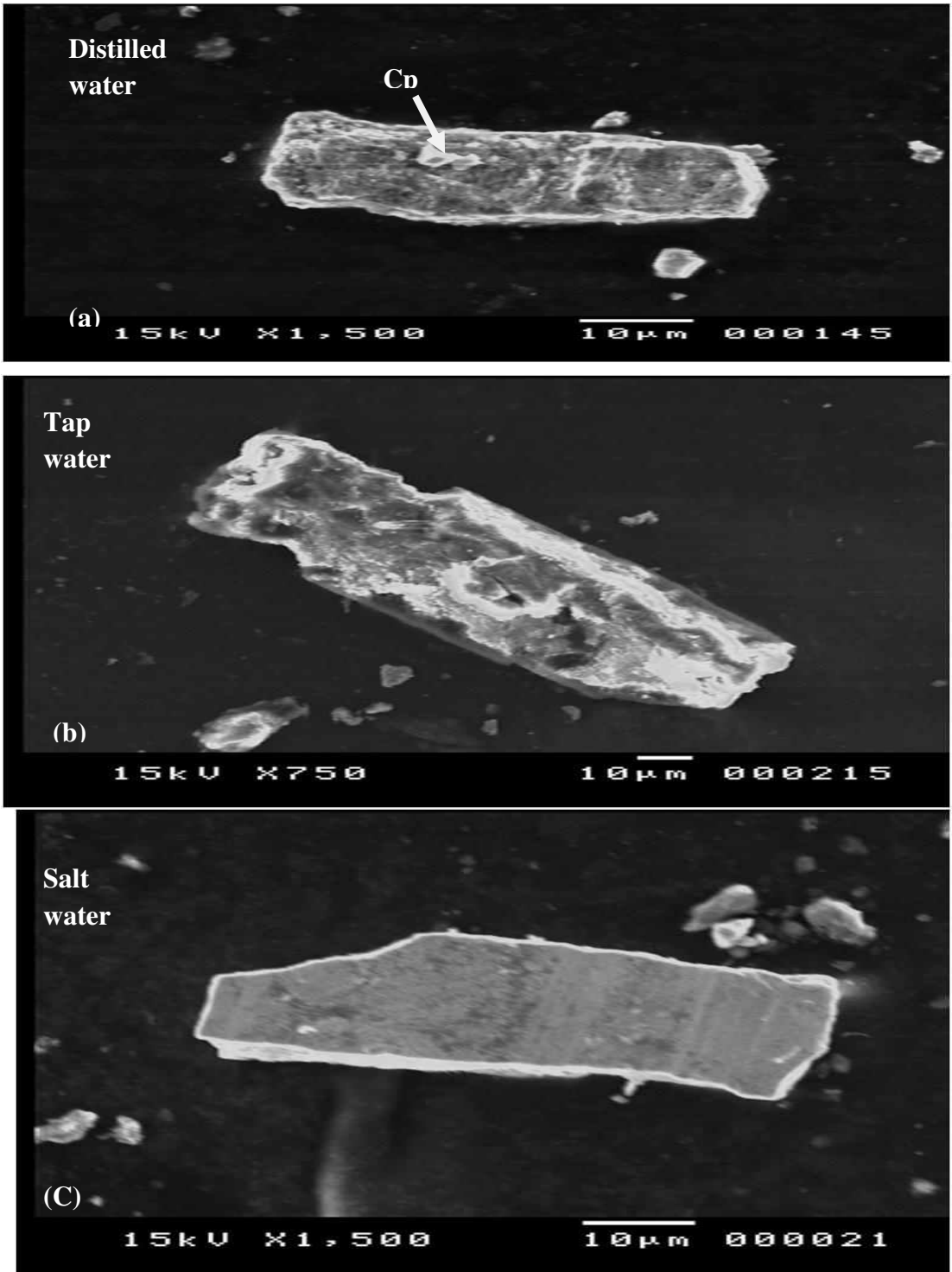
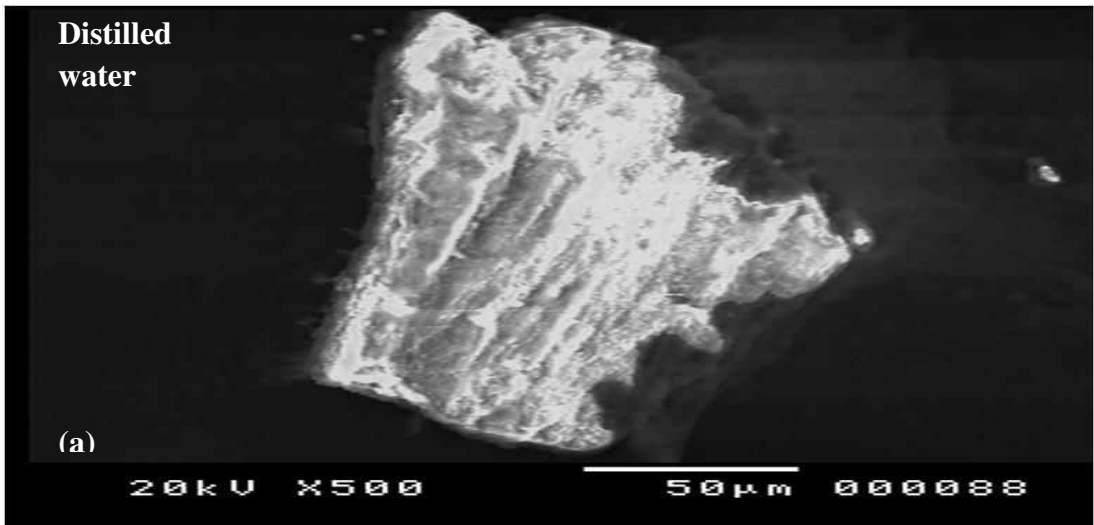
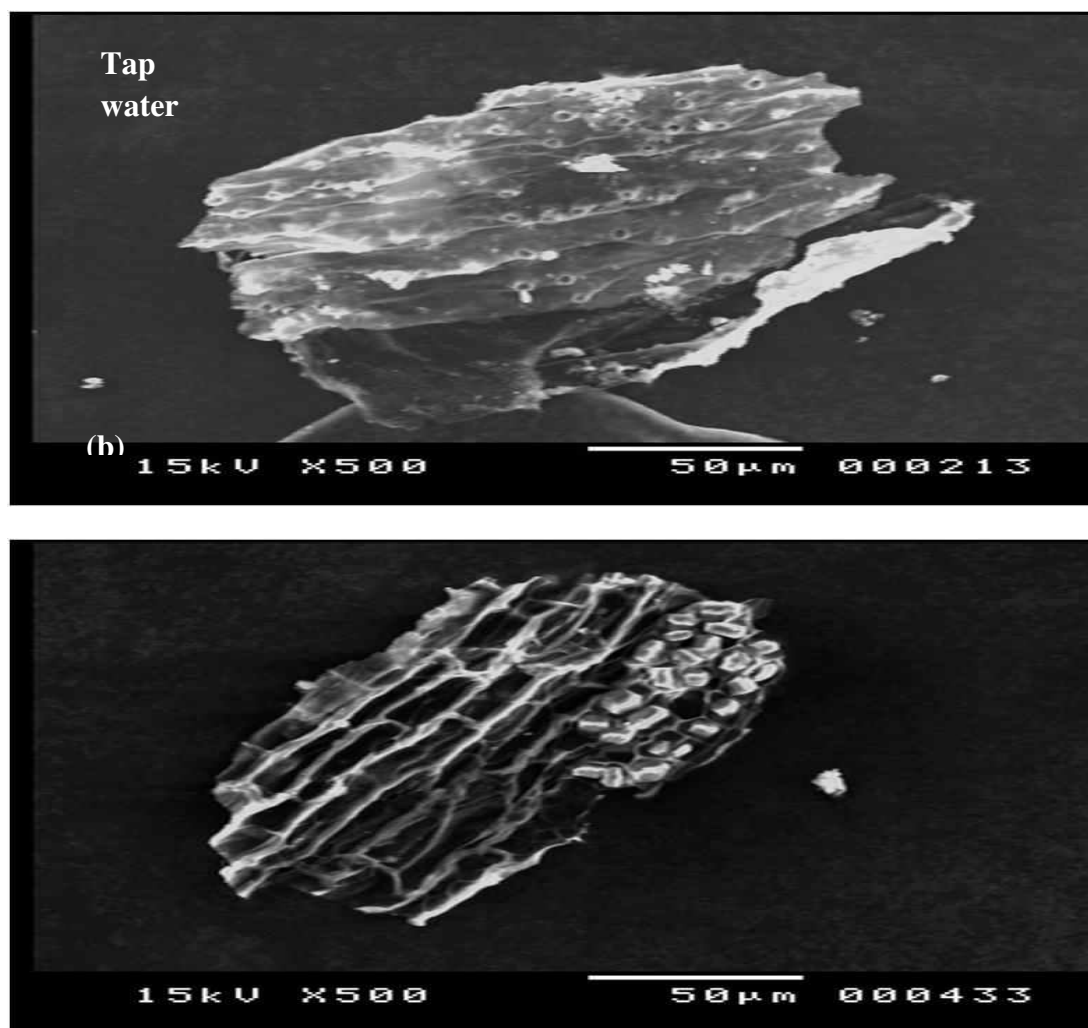


Fig. 8, SEM photos illustrating typical particles cavitating in different waters

Under microscopic examination, the most striking features of many of the fracture faces caused by fatigue crack is the presence of distinct line markings, parallel to each other and normal to the direction of crack growth. These lines generally called striations. Each striation corresponds to one stress cycle, and the distance between striations is the amounts that crack have moved forward during that cycle [4, 35]. Since the particles are the negative replica for the eroded surface, it is expected to observe the striations on particles surface as shown in Fig.9. The particles developed for salt water shown in Fig. 9-c are different from those for distilled water and tap water shown in Fig. 9(a, b), respectively. This is due to severe corrosive action of salt water, where the corresponding action makes dissolution for a phase of material (ferrite). It can also be observed that the corrosion product formed on the surface of particles labeled C<sub>p</sub>. All the particles characteristics aforementioned give evidence that they were developed by fatigue cracks. On the other hand, such large particle size, that is in the range of 200 μm or more, cannot be successfully described by microjet, therefore these particles were developed from long cracks, which are most likely caused by extremely high shock pressure emitted from the collapsing of bubble clusters. This result is in agreement with results reported by Ahmed et al. [4] and Abouel-kasem et al. [7], that the important mechanism to transfer the cavitation energy to the solid is by shock pressure accompanied by collapsing massive bubbles.



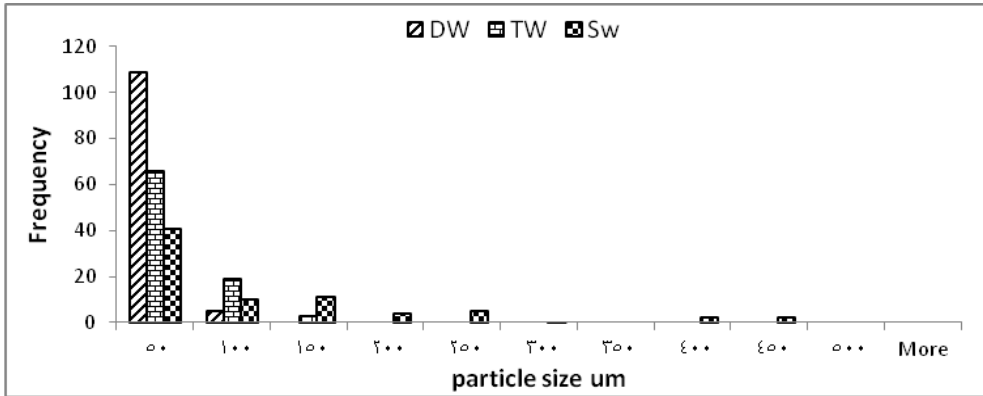


**Fig. 9. SEM photos illustrating cavitating particles in different waters with cycle striations stress**

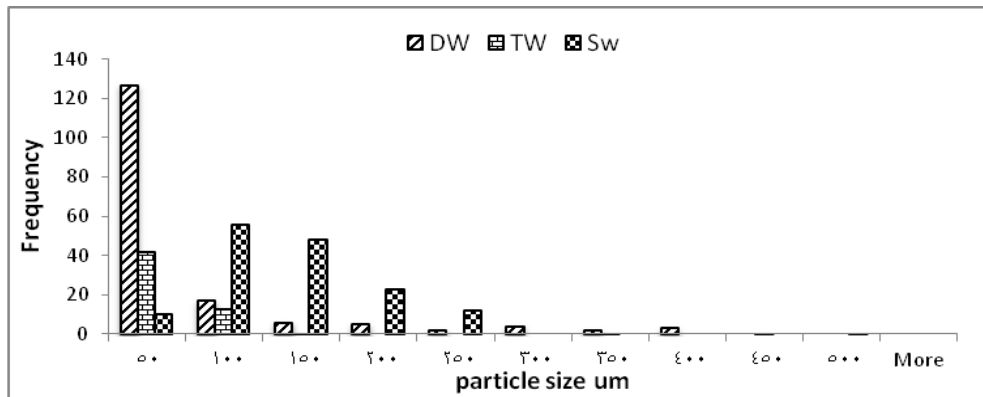
### *3.2 Particle size distribution*

For quantitative morphological analysis, such as size, perimeter and roundness, low SEM magnification images were used. The quantitative morphological analysis was measured for more than 50 particles for each test solution and time. Since most of the particles, produced by cavitation erosion, have an irregular shape as illustrated in Sec. 3.1 the equivalent diameter of the projected area has been used to represent the size of wear particles. The equivalent diameter of the projected area is the diameter of a circle having the same area of the projected area of the particle in its stable orientation. In this work, the size is only considered for the characterization; since in previous study by one of the authors [27], it was found that the shape factors could not be significantly discriminate between the particles produced in water and oil-water emulsions.

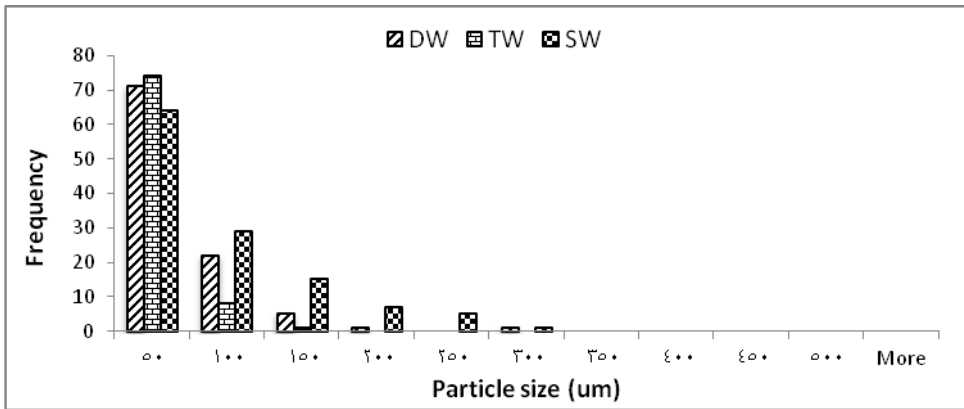
Figure 10 shows the distribution of the particle size for distilled water, tap water and salt water for test time of 20, 30, 40, and 50 min. It can be observed that for each test solution, the particles have large and smaller sizes. However, the size range depends on the test solution. For distilled and tap water, the frequency of particle size distribution was the larger for small sizes, about 50  $\mu\text{m}$ , than that for salt solution. However, for salt water the frequency distribution of particle size larger than 50  $\mu\text{m}$ , was the dominant. This indicates that the corrosion enhances the erosion in removing the large particles. This enhancement will be clarified in the next section.



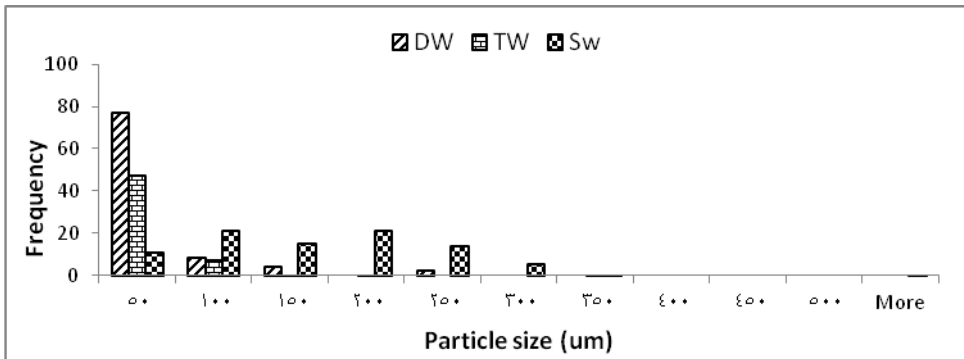
a-



b-



c-



d-

Fig.10 Frequency distribution of particle size after cav. erosion in different corrosive media (DW,TW,SW) , a)20min, b)30min, c)40min, d)50min

### 3.3 Effect of Corrosion on Cavitation Damage

When cavitation attack takes place in aggressive media, both mechanical erosion and electrochemical corrosion coexist and they may interact synergistically to aggravate the attack on the material. As proposed by many researchers, this synergistic effect is due to the enhancement of corrosion by erosion and/or enhancement of erosion by corrosion [13]. The synergism was not well understood from the view of damage behavior. Figure 11 shows photos for particles in salt waters. It is easy to see the effect of corrosion on the surface of these particles, where many black dents, voids and/or pits were formed as result of the dissolution of ferrite phase. With time, as observed by Karrab et al. [16], these sites coalesce giving rise to many cracks to develop, as labeled C in Fig. 11(a). This gives evidence that the corrosion dents acts as favorite sites for stress concentration and initiation of cracks.

Another effect of corrosion on developing cavitation damage is the formation of many cracks along ferrite-pearlite grain boundaries as shown in Fig.12. This lets another faces such as pearlite unable to withstand the moderate blow of emitted shock waves and consequently many particles fall off. These two effects of corrosion in salt

water aggravate the cavitation attack and shorten the incubation period of the tested material in comparison with the distilled water and tap water as shown in figure 13.

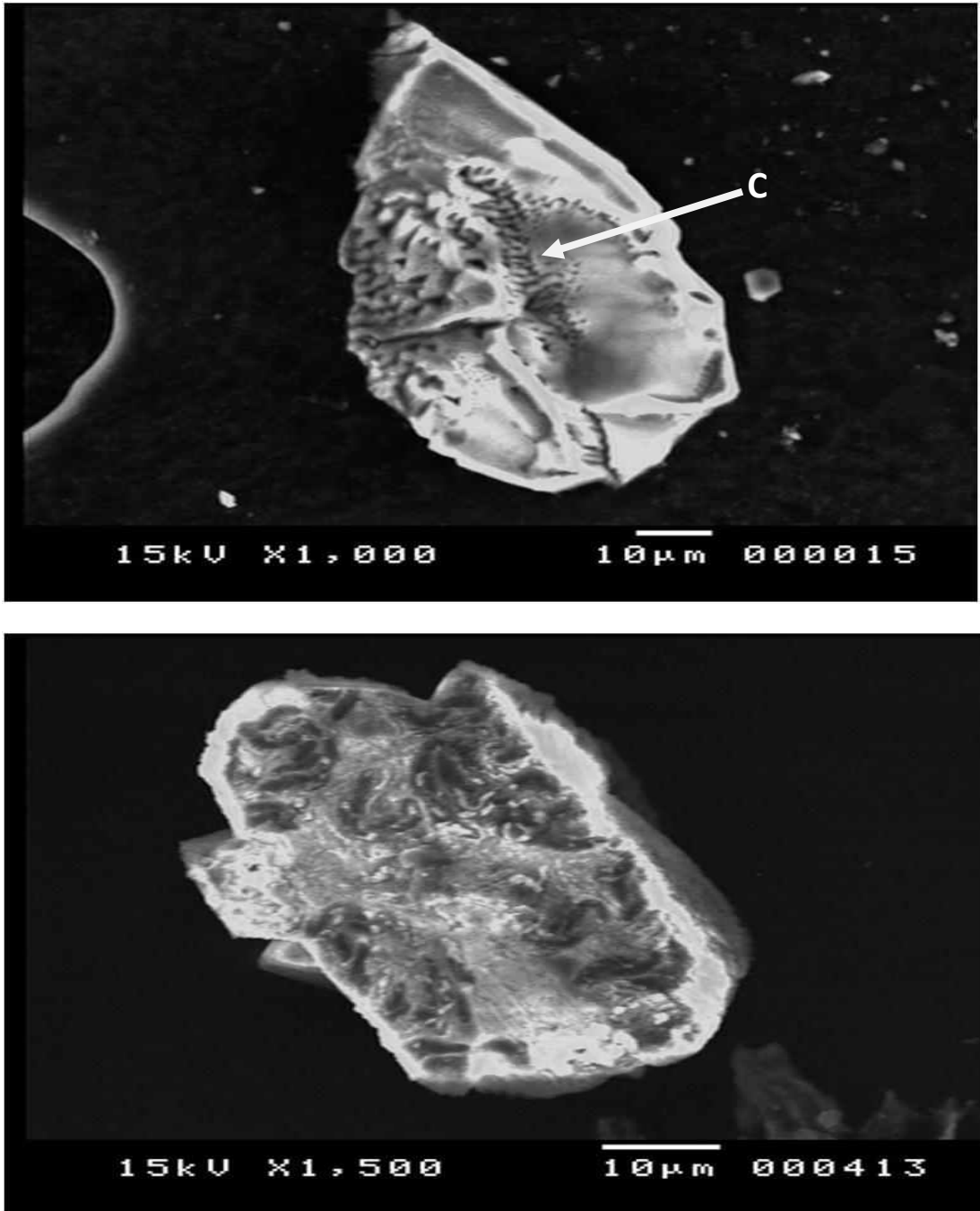


**Fig. 11, SEM photographs showing formation of many cracks along Ferrite-Pearlite grain boundaries.**

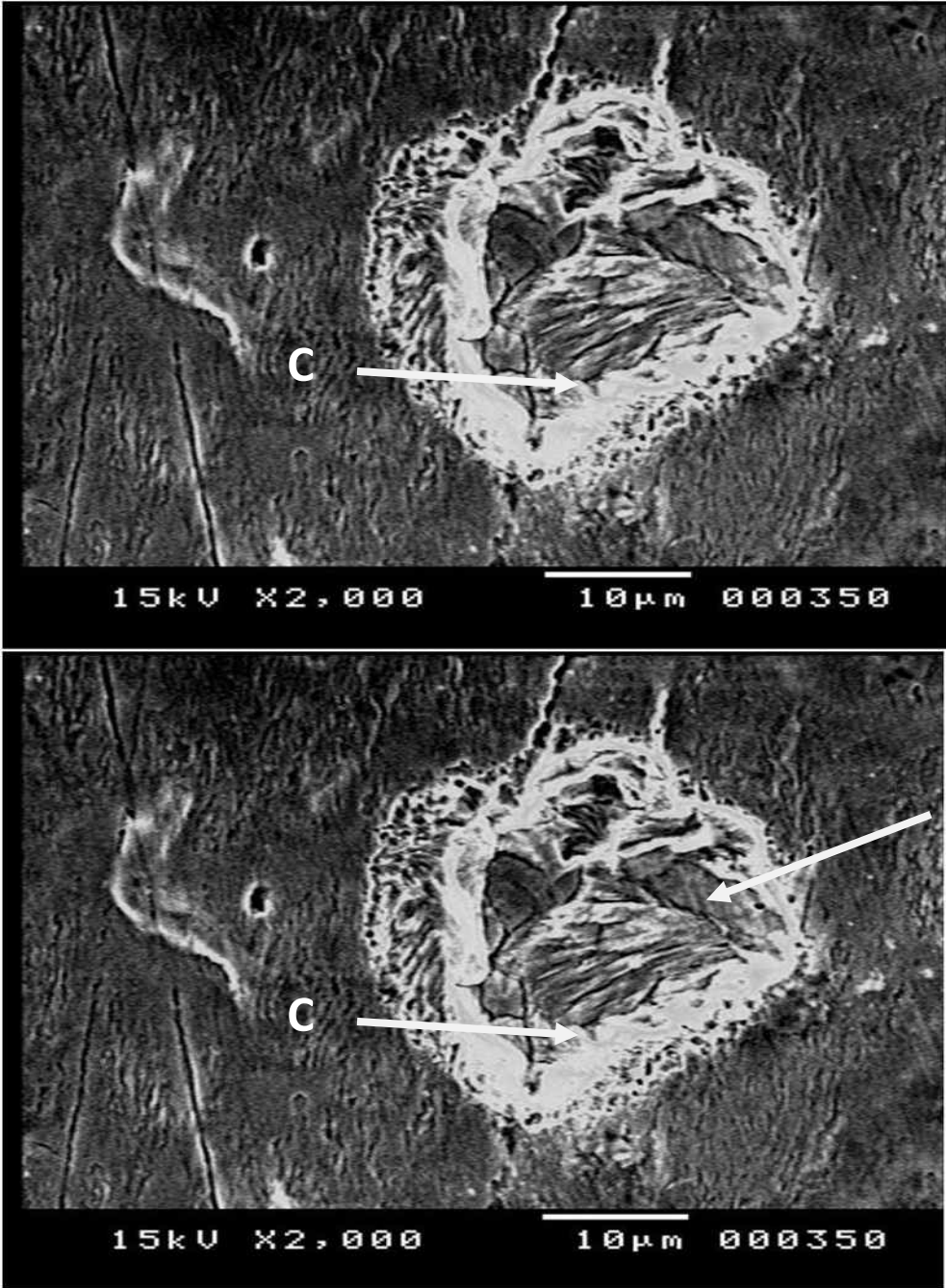


Fig. 12. SEM photographs showing formation of many cracks along Ferrite Pearlite grain boundaries

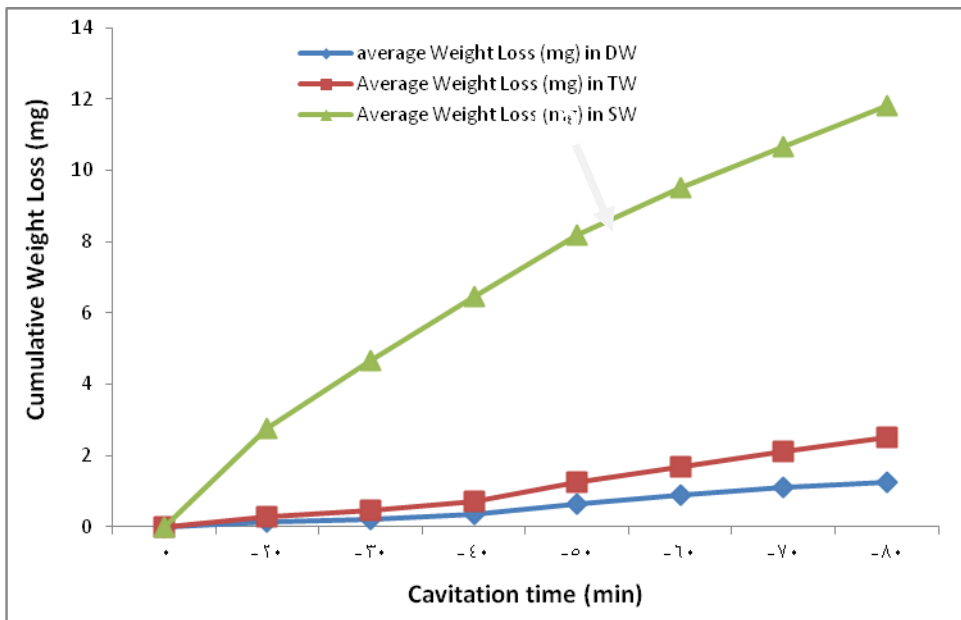


Fig. 13. Cumulative weight loss with test time in the three test liquids

#### 4. Conclusions

1. The role of corrosion in the development of cavitation erosion appears clearly in the case of salt water where the dissolution of ferrite helps in the initiation of cracks in regions of the ferrite as well as the boundary of ferrite-pearlite.
2. The size of particles and their shape, which is irregular, are comparable for all test solutions, which means that erosion is dominant.
3. The morphological features such as ridges, crack propagation marks and secondary cracks shown on the particle surface illustrate that the cavitation erosion mechanism is fatigue failure irrespective of test solution.
4. The frequency distribution graph of particles shows clear domination of distilled and tap water for sizes small sizes (<50  $\mu\text{m}$ ) whereas salt water particles were dominant for larger sizes (>50  $\mu\text{m}$ ). i.e. the corrosion enhances the erosion in removing the large particles.

#### 5. References:

- [1] Preece, C. M., and Hansson, I. L. H., "A metallurgical approach to cavitation erosion. Advances in the mechanics and physics of surfaces" Vol. 1, R. M. Latanision and R. J. Courtel, eds., Harwood Academic, (1981), pp. 199–253.
- [2] Woytowicz, P. J. and Richman, R. H., "Solid mechanics modeling of erosion damage, applications of continuum damage mechanics to fatigue and fracture" ASTM STP 1315, D.L. McDowell, Eds., American Society for Testing and Materials, (1997), pp.186–199.

- [3] Ahmed, S. M., Hokkirigawa, K., Oba, R., and Kikuchi, K. "SEM observation of vibratory cavitation fracture-mode during the incubation period and the small roughness effect" *JSME Int. J., Ser. II*, **34**(3), (1992), pp. 298.
- [4] Ahmed, S. M., Hokkirigawa, K., and Oba, R., "Fatigue failure of SUS 304 caused by vibratory cavitation erosion" *Wear*, **177**, (1994), pp. 129–137.
- [5] Ahmed, S. M., "Investigation of the temperature effects on induced impact pressure and cavitation erosion" *Wear*, **218**, (1997), pp.119–127.
- [6] Abouel-Kasem, A., and Ahmed, S. M., " Cavitation erosion mechanism based on analysis of erosion particles" *Trans. ASME, J. Tribol.*, **130**, (2008), pp. 031601-(1-6).
- [7] Abouel-Kasem, A. Ezz El-Deen, K.M. Emar, Ahmed, S.M., "Investigation into cavitation erosion pits" *ASME, J. Tribol.*, **131**, (2009), pp. 031605-1-031605-7.
- [8] Saleh, B., Abouel-Kasem, A., Ezz El-Deen, A., Ahmed, S.M., "Investigation of temperature effects on cavitation erosion behavior based on analysis of erosion particles" *Trans. ASME, J. Tribol.*, **132**, (2010), pp. 031601.
- [9] Preece, C.M., " Cavitation erosion. Treatise on materials science and technology" Academic Press; New York. **16**, (1979), pp. 249.
- [10] Okada, T., "Corrosive liquids effects on cavitation erosion" *J. Ship Res.*, **25**(4), (1981), pp. 271-284.
- [11] Wood, R.J.K. and Fry, S.A., "The synergistic effects of cavitation erosion and corrosion for copper and cupro-nickel in sea water" *J. Fluid Eng.*, **111**, (1989), pp. 271-277.
- [12] Tomlinson, W.J. and Talks, M.G., "Cavitation erosion of grey cast irons containing 0.2 and 1.0% phosphorous in corrosive waters" *Trib. Int.*, **22**, (1989), pp. 195-204.
- [13] Kwok, C.T., Cheng, F.T., Man, H.C., "Synergistic effect of cavitation erosion and corrosion of various engineering alloys in 3.5% NaCl solution" *Mat. Sci. Eng.*, **A290**, (2000), pp.145–154.
- [14] Al-Hashem, A., Tarish, H. and Akbar, A., "Cavitation corrosion behavior of carbon Steel, al-bronze and cobalt-based alloy in seawater" *Corrosion Conf., NACE Int.* (2007)
- [15] Zhao, M., Wang, J., Chen, D., Hao, X., Wang, B., "The difference between synergistic erosion-corrosion and corrosion of mild steel in SiC suspension" *J. Alloys and Compounds*, **466**, (2008), pp. 421–428.
- [16] Karrab, S.,A., Doheim, M. A., Ahmed, S.M., Mohamed S. M., "Study of cavitation erosion pits on 1045 carbon steel surface in corrosive waters" *Trans. ASME, J. Tribol* **134**, (2012), pp. 011602
- [17] Karrab, S.,A., Doheim, M. A., Ahmed, S.M., Mohamed S. M., "Investigation of the ring area formed around cavitation erosion pits on the surface of carbon steel" *Tribol Lett.*, **45**, (2012), pp. 437–444.
- [18] Chen, H., Li, J., "A ring area formed around the erosion pit on 1Cr18Ni9Ti stainless steel surface in incipient cavitation erosion" *Wear*, **266**, (2009), pp. 884–887.
- [19] Chen, H., "Iridescent rings around cavitation erosion pits on surface of mild carbon steel" *Wear*, **269**, (2010), pp. 602–606.
- [20] Neale, M.J., " Tribology handbook" 2<sup>nd</sup> ed., Elsevier; (1995)

- [21] Hunt, T.M., “ Handbook of wear debris, analysis and particle detection in liquids” Elsevier, Essex, UK. (1993)
- [22] Sperrin, T.P., Nowell, T.T., “ SYCLOPS- A qualitative debris classification system developed for RAF early failure detection centers” Trib. Int., **38**, (2005), pp. 898-903.
- [23] Kenkermath, D., Thiruvengadam, A., “Analysis and characterization of particles produced by cavitation erosion” In: Proc. Conf. Cavi., 1 Mech. E, Edinburgh, (1974), pp. 285–95.
- [24] Tomlinson, W.J., Chapman, D., “Effect of amplitude on the erosion and corrosion of copper by 20 kHz ultrasound” Wear, **27**, (1974), pp. 381–4.
- [25] Ahmed, S.M., Hokkirigawa, K., Kikuchi, K., Higuchi, J., Oba R., “SEM studies of particles produced by cavitation erosion” JSME, Int. J. Ser B, **3624**, (1993), pp. 517–23.
- [26] Hattori, S., Nakao E., “Cavitation erosion mechanism and quantitative evaluation based on erosion particles” Wear, **249**, (2002), pp. 839–45.
- [27] Abouel-Kasem, A., Baha, S., and Ahmed, S. M., “Quantitative analysis of cavitation erosion particle morphology in dilute emulsions” Trans. ASME, J. Tribol., **130**, (2008), pp. 041603-1.
- [28] Abouel-Kasem, A., Emara, K. M., and Ahmed, S. M., “Characterizing cavitation erosion particles, by analysis of SEM images” Trib. Int., **42**, (2009), pp. 130-136.
- [29] Knapp, R.T., Daily, J.W., and Hammitt, F.G., “Cavitation, McGraw-Hill, New York. (1970)
- [30] Hammitt, F. G., “Cavitation and multiphase flow phenomena” McGraw-Hill, New York. (1980)
- [31] Vyas, B. and Preece, C.M., “Stress produced in a solid by cavitation” J. Appl. Phys., **47**(2), (1976), pp. 5133-5138.
- [32] ASTM G 32-09, “ Standard test method for cavitation erosion using vibratory apparatus” Annual book of ASTM standards, ASTM, Philadelphia, PA, (2009)
- [33] Takasaki, S. and Yamada, Y., “Effects of temperature and aggressive anion on corrosion of carbon steel in potable water” Corrosion Science, **49**, (2007), pp. 240-247.
- [34] Davis, J. R., Mills, K. M., Lampman, S. R., “ Metals handbook. 10<sup>th</sup> Edition Vol. 1. Properties and selection: Irons, steels, and high-performance alloys” ASM International, Materials Park, ISBN: 0-87170-378-5 and 0-87170-377-7, (1990), pp. 1063.
- [35] Pook, L.P and Smith, R. A., “Theoretical background to elastic fracture mechanics, current status, fracture prospects” In Smith ed., Proc. Cambridge Univ. Conf. (1979)

## List of Figures

- Fig.1. a schematic diagram of the test equipment.
- Fig.2. SEM photograph showing the microstructure of steel AISI-1045 with (white) pearlite and (dark) ferrite.
- Fig. 3. Schematic diagram of the ferrograph.
- Figure 4, SEM photos illustrating dominant salt crystal over cavitated particles in salt solution.

- Fig. 5. SEM photo illustrating crystallization of NaCl crystals over the cavitated particles
- Fig. 6, SEM Photographs of particles removed for 1045 carbon steel cavitating in different water at test time of 20 min.
- Fig.7, SEM photographs of particles from 1045 carbon steel cavitating in different waters and at test time of 30 min.
- Fig. 8, SEM photos illustrating typical particles cavitating in different waters.
- Fig. 9, SEM photos illustrating cavitating particles in different waters with stress cycle striations.
- Fig.10. shows the distribution of the particle size for distilled water, tap water and salt water for test time of 20, 30, 40, and 50 min.
- Fig. 11. SEM monographs showing cavitated particles in salt waters.
- Fig. 12. SEM photographs showing formation of many cracks along Ferrite-Pearlite grain boundaries.
- Fig. 13. Cumulative weight loss with test time in the three test liquids

### اختبار شكل الحبيبات اثناء عملية التآكل التكهفي في المياه التآكلية

ثم تحليل ودراسة جزيئات التآكل الناتجة من اختبارات التآكل التكهفي على الصلب الكربوني نوع 45 حسب مواصفات المعهد الامريكي للحديد والصلب (AISI) في ثلاث بيئات تآكلية مختلفة ابتداء من الماء المقطر ثم الماء العذب او ماء الشرب ثم الماء المالح وهو عبارة عن ماء مقطر مع ملح كلوريد الصوديوم بتركيز 3% ، حيث تم استخدام المجهر الالكتروني وتكوين قاعدة بيانات لمزيد من التحليل. أظهرت الدراسة انه ليس هناك فرق ملحوظ في حجم الحبيبات مع تغير محلول الاختبار ومع ذلك حدث اختلاف في التوزيع التكراري لحجوم الحبيبات باختلاف محلول الإختبار ، حيث لوحظ أن التوزيع التكراري لحجوم الحبيبات كان الأعلى في الحجوم الصغيرة للمياه العذبة والمياه المقطرة اما في حالة الماء المالح ، فإن التوزيع التكراري كان الأعلى للأحجام الأكبر (أكبر من 50 ميكرومتر) . كما لوحظ أن كل الجسيمات بغض النظر عن محلول الاختبار أظهرت ميّزات تشكيلية (مورفولوجية) مثل الشكل الرقائقّي و انتشار الشقوق على سطح الجسيمات والشقوق الثانوية وهذا يشير إلى أن تم إنتاج الجزيئات من خلال آلية واحدة، ألا وهي الكلال. وفيما يتعلق بدور التآكل في تطوير تآكل التكهف، كان أكثر وضوحا في حالة المياه المالحة. ووجد أن إذابة طور الفريت تعمل كمناطق لتركيز الإجهاد التي تؤدي الى استحداث تشققات .